Relationship between magnetoresistance behavior and magnetic states in intercalated compounds Fe$_x$TiS$_2$

N. V. Selezneva [1], E. M. Sherokalova [1], A. Podlesnyak [2], M. Frontzek,[2] and N. V. Baranov [1,3,*]

[1]*Institute of Natural Science and Mathematics, Ural Federal University, 620083 Ekaterinburg, Russia*

[2]*Neutron Scattering Division, Oak Ridge National Laboratory, Oak Ridge, Tennessee 37831, USA*

[3]*M.N. Miheev Institute of Metal Physics, Ural Branch of the Russian Academy of Science, 620108 Ekaterinburg, Russia*

Temperature and field-dependent neutron powder diffraction (NPD) measurements have been performed to reveal the nature of the unusual evolution of the magnetoresistance behavior with increasing Fe content in the intercalated compounds Fe$_x$TiS$_2$ (with $x = 0.25$, 0.33, 0.50, 0.55) synthesized by solid-phase reaction method with prolonged homogenization heat treatment. As derived from neutron diffraction measurements, both the Fe$_{0.25}$TiS$_2$ and the Fe$_{0.50}$TiS$_2$ compound exhibit an antiferromagnetic (AFM) order below their respective Néel temperatures $T_N \approx 52$ K and $T_N \approx 140$ K, which results in the presence of a large magnetoresistance accompanying the field-induced phase transition from AFM to the ferromagnetic (FM) state. At low temperatures, this AFM-FM transition is irreversible, confirmed by the irreversibility of changes in the NPD patterns and the presence of remnant magnetoresistance. In contrast, Fe$_{0.33}$TiS$_2$ shows short-range magnetic order at $T_f \approx 44$ K due to a triangular network of intercalated Fe atoms and frustrations of exchange interactions with a field-induced FM alignment of Fe magnetic moments in an applied magnetic field as revealed by NPD measurements. The field-induced transformations of the cluster glass magnetic state in this compound lead to a significant decrease in electrical resistivity. According to NPD data, a reduced impact of an external magnetic field on the electrical resistivity of the compound Fe$_{0.55}$TiS$_2$ can be ascribed to the presence of ferromagnetic or ferrimagnetic order in compounds with the Fe concentrations above $x = 0.50$. The results obtained indicate that the distribution of the Fe atoms, along with their concentration in Fe$_x$TiS$_2$ layered compounds, plays a decisive role in the formation of the magnetic state and the behavior of the magnetoresistance.

I. INTRODUCTION

Transition metal dichalcogenides MX_2 with a layered crystal structure where hexagonal layers of transition (M) metal are sandwiched between two hexagonal layers of chalcogen (X) atoms have attracted relentless interest owing to the rich variety of unusual properties and potential applications [1–6]. Among other phenomena such as the formation of a charge density wave and superconductivity [7–9], the magnetoresistance (MR) of materials based on MX_2 is receiving increasing attention [10], as it reflects the physical mechanisms of electron transport in such quasi-two-dimensional systems subjected to magnetic fields, and can be used in various devices. The discovery, understanding, and design of new material exhibiting large magnetoresistance for applications remain hot topics in condensed matter physics. The nature of MR, which is defined as $\Delta\rho/\rho = \{[\rho(H) - \rho(0)]/\rho(0)\}$ and is specified as a percentage, may vary from material to material. An analysis of the experimental data shows that the magnetotransport is intrinsically different for electrons within magnetic and nonmagnetic materials; two types of magnetoresistance behavior can be distinguished: positive MR and negative MR. An extremely large and positive nonsaturating MR was observed in MTe$_2$($M = $ W, Hf, Mo) crystals that do not exhibit a magnetic order [10–13]. Generally, the occurrence of positive MR in the materials without magnetic order can be explained by the Lorentz contribution to the excess resistivity. A very large positive MR in the semimetallic WTe$_2$ is explained by the balanced electron-hole populations [10,11].

Magnetically ordered materials can demonstrate negative or positive MR depending on the measuring geometries (the orientations between the magnetic field and current relative to the crystallographic axes) as well as on the arrangement of the magnetic moments (see Refs. [14,15], for instance). An enhanced value of the positive MR ($\Delta\rho/\rho$ up to 60% at 2 K) was detected in single crystalline samples of Fe intercalated ferromagnetic compounds Fe$_x$TaS$_2$ ($0.23 \leqslant x \leqslant 0.35$) in the vicinity of the coercive field [16,17]. However, antiferromagnetically ordered compounds Fe$_x$TiS$_2$ with Fe concentrations $x \sim 0.25$ and $x \sim 0.50$ were found to exhibit large negative MR values [18–21], which was ascribed to the superzone mechanism [22].

According to the superzone model [22], the electrical conductivity of the metallic antiferromagnet can be described as $\sigma_{ij} = 1/\rho_{ij} = \sigma_{ij}^0(1 - \delta)$, where σ_{ij}^0 is the conductivity of the metal with nondeformed Fermi surface, $\delta = \Gamma m$ is proportional to the width of the energy gap at the boundaries of the new Brillouin zones (superzones), m is normalized magnetization, and Γ depends on the exchange integral between the

---

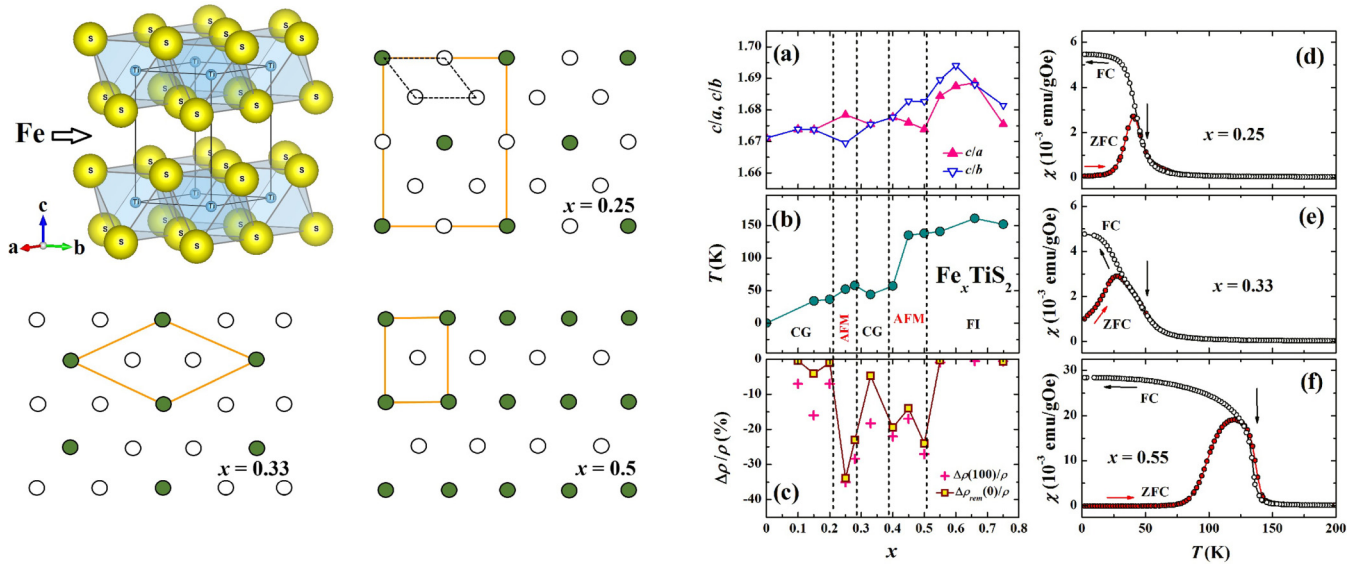*Corresponding author: baranov@imp.uran.ru

FIG. 1. Overall crystal structure of TiS_2 and top view with iron atom positions in octahedral sites in Fe_xTiS_2 at various Fe concentrations as labeled (left panel). Dashed line shows the primitive hexagonal cell of the parent ($x = 0$) compound and solid line indicates the possible supercells formed by intercalated atoms. Middle panel shows (a) concentration dependencies of the ratio of the lattice parameters c_0/a_0 and c_0/b, (b) magnetic ordering temperature, and (c) magnetoresistance $\Delta\rho_{100}/\rho$ measured at $T = 4$ K in the 100 kOe field (crosses) and remnant magnetoresistance $\Delta\rho_{rem}/\rho$ (squares) for Fe_xTiS_2 (a_0 and c_0 are the primitive hexagonal unit cell parameters of the NiAs structure). Right panel shows temperature dependencies of the magnetic susceptibility for the samples with $x = 0.25$ (d), $x = 0.33$ (e), and $x = 0.55$ (f) measured in ZFC and FC regimes. Magnetic and MR data are taken from Ref. [20].

conduction electrons and localized electrons ($3d$ electrons of iron in our case). Γ includes the contributions from all new magnetic superzone boundaries cutting the Fermi surface of an antiferromagnetically ordered metal. The zeroing of δ due to the disappearance of energy gaps at the boundaries of superzones during field AFM-FM transitions is assumed to lead to significant MR in Fe_xTiS_2 at $x \sim 0.25$ and $x \sim 0.50$. The presence of a large remnant magnetoresistance was proposed to be considered as an indicator of the irreversibility of the AFM-FM transition [18–21].

The Fe_xTiS_2 system is unique among intercalated systems because it exhibits an unusual combination of magnetic, transport, and hysteresis properties, as well as field-induced phase transitions [19,20,23]. The magnetic behavior of Fe_xTiS_2 is found to be characteristic of Ising systems [19,24,25]. This is supported by the observation of a large (up to $\sim 0.6\mu_B$) unquenched orbital moment of Fe ions [26,27]. A sketch of the crystal structure and the changes in the crystal, magnetic, and magnetoresistive characteristics with Fe content in this system are shown in Fig. 1. The magnetic and magnetoresistive behavior of Fe_xTiS_2 with $x < 0.20$ is quite characteristic for cluster spin glasses (CG) with Ising spins, and freezing temperature expectedly increases with growth of the Fe content up to ~ 50 K [20,28]. From the observation of a large remnant magnetoresistance the magnetic order of $Fe_{0.25}TiS_2$ was suggested as antiferromagnetic (AFM) [20,21], as is confirmed by neutron diffraction measurements presented in this manuscript. As can be seen in Fig. 1(c), an absolute value of the remnant MR $\Delta\rho_{rem}/\rho = \{[\rho_{fin}(0) - \rho_{vgn}(0)]/\rho_{vgn}\} \times 100$ reaches about 35% at $x = 0.25$ [ρ_{vgn} is the initial value of the electrical resistivity at $H = 0$ in the virgin magnetic state obtained after cooling the sample in zero field to a given

temperature; $\rho_{fin}(0)$ is the final value of the electrical resistivity after preliminary magnetization and switching off the magnetic field]. The magnetic behavior of the Fe_xTiS_2 compounds with $x \sim 0.33$ was classified as of the CG type [20]. The absence of long-range magnetic order in $Fe_{0.33}TiS_2$ was confirmed by preliminary neutron diffraction measurements. It was suggested that the CG magnetic state in this compound results from the frustration of exchange interactions of different signs. Apparently due to such frustrations the freezing temperature for $Fe_{0.33}TiS_2$ is lower ($T_f \approx 44$ K) than the magnetic ordering temperature of the compounds with $x = 0.25$ and $x = 0.28$, i.e., with lower Fe concentrations [see Fig. 1(b)].

Unlike the cluster glass-like magnetic behavior at $x \approx 0.33$, the Fe_xTiS_2 compounds with $x \approx 0.50$ exhibit AFM order with elevated Néel temperatures ($T_N \approx 135$–140 K) and large values of the remnant MR ($\Delta\rho_{rem}/\rho \approx -35\%$). The presence of the remnant MR in $Fe_{0.50}TiS_2$ was explained by the field-induced phase transition from AFM to the metastable ferromagnetic (FM) state, which was evidenced by neutron diffraction data [18]. As can be seen in Fig. 1, no remnant MR and low $|\Delta\rho/\rho|$ values in high magnetic fields (less than 1%) were observed in compounds with Fe content above $x = 0.50$, which was ascribed to the possible appearance of the ferrimagnetic order in compounds with $x > 0.50$ due to the Fe-Ti mixing in cationic layers [20]. The change in the magnetic critical temperatures presented in Fig. 1(b) are consistent with literature data (see Ref. [20] and references therein).

The Fe_xTiS_2 system seems to exhibit a set of various magnetic states as well as different behaviors of magnetoresistance. The present work aims to establish or confirm magnetic orderings at various Fe concentrations, as well as elucidate

how changes in the magnetic state with Fe concentration and magnetic field affect magnetoresistance. There is a consensus in the literature regarding the spin-glass and cluster-glass magnetic states in compounds with low iron content. Therefore, in this work, we focused on compounds with $x > 0.20$, for which the MR behavior changes dramatically with Fe concentration. We carried out neutron diffraction measurements on these samples and analyzed the changes in the magnetic structure and magnetoresistance at various temperatures and magnetic fields. Comparative study and analysis of neutron diffraction, magnetization, and magnetoresistance provide a deeper understanding of the underlying physics. This will also help to optimize the MR materials and to use the MR measurements for the characterization of the magnetic states.

II. EXPERIMENT

To obtain polycrystalline Fe_xTiS_2 samples with Fe concentrations within the range $0.25 \leqslant x \leqslant 0.55$, the initial TiS_2 compound was first synthesized by heat treatment of a mixture of starting materials (titanium with a purity of 99.95% and sulfur with a purity of 99.99%) at $800\,°C$ for one week in an evacuated quartz tube. Then, mixtures of Fe powder (99.98% purity) and TiS_2 powder were pressed into cylindrical tablets and annealed under the same conditions. Then, the obtained samples were ground, compacted again into tablets, and then homogenized inside a sealed quartz tube for two weeks at $800\,°C$, followed by cooling by removing the ampule from the furnace into the air. The monitoring of changes in the phase composition during the synthesis, as well as the determination of the structural characteristics of the final products, was carried out using a Bruker D8 Advance x-ray diffractometer with Cu K_α radiation. The chemical composition of the synthesized samples was checked by using a Carl Zeiss AURIGA Crossbeam Workstation equipped with energy dispersive x-ray spectrometer. The measurements of the magnetic susceptibility and magnetization in magnetic fields up to 70 kOe were performed by means of a SQUID MPMS magnetometer (Quantum Design, USA) in the temperature interval from 2 K up to 350 K. Neutron powder diffraction (NPD) data were collected on the Wide-Angle Neutron Diffractometer (WAND^2) installed at the HB-2C beam port of the High Flux Isotope Reactor (HFIR) at Oak Ridge National Laboratory (ORNL), USA, and employing Ge (113) reflection to produce a monochromatic neutron beam with a wavelength of $\lambda = 1.482$ Å [29]. A vertical field cryomagnet was used for measurements in magnetic fields up to 50 kOe and in the temperature range from 2 up to 200 K. The neutron powder diffraction measurements on the $Fe_{0.50}TiS_2$ sample were performed at the DMC diffractometer at the Spallation Source SINQ, Switzerland with neutron wavelength $\lambda = 3.8$ Å in magnetic fields up to 28 kOe [18]. The tablets of the compacted powder sample were loaded into a vanadium can. Crystal and magnetic structure refinements were performed by the Rietveld method with the program FULLPROF [30]. The transversal magnetoresistance of Fe_xTiS_2 was measured on parallelepiped samples with sizes of about $2 \times 2 \times 8$ mm^3 made from pellets by a four-contact ac method using a cryofree DMS-1000 system (Dryogenic Ltd, UK) in magnetic fields up to 100 kOe.

III. RESULTS AND DISCUSSION

Further analysis of the x-ray data obtained in our previous work [20] shows that the ratios of the lattice parameters c_0/a_0 and c_0/b slightly increase with Fe intercalation up to $x \sim 0.20$ (a_0 and c_0 are the primitive hexagonal unit cell parameters of the NiAs structure). However, these ratios are equal to each other [Fig. 1(b)], indicating that the hexagonal arrangement of chalcogen and Ti ions in the ab plane is retained and the structure can be described by the same space group $P\bar{3}m1$ as the initial compound TiS_2 ($x = 0$). As shown in Ref. [20], the unit cell volume increases with increasing Fe concentration in Fe_xTiS_2, which is consistent with earlier studies [28,31]. The Fe atoms located in octahedral sites between S–Ti–S sandwiches do not have a long-range order below $x \sim 0.20$, although electron microscopy studies have recently shown [32] that some short-range Fe order can be observed even at $x = 0.15$. Further intercalation is accompanied by the formation of various orderings of Fe atoms and superstructures, as displayed on the left panel of Fig. 1. An increase in the Fe content up to $x = 0.25$ is accompanied by the appearance of a difference between the c_0/a_0 and c_0/b values and monoclinic structure (space group $C12/m1$) due to the formation of the Fe chains and the $2\sqrt{3} \times 2 \times 2$ NiAs superstructure. The difference between c_0/a_0 and c_0/b indicates that the hexagonal arrangement of chalcogen and Ti atoms in the ab plane is somewhat distorted at $x = 0.25$. In the concentration range $0.28 \leqslant x \leqslant 0.40$, the compounds do not exhibit monoclinic structure and the c_0/a_0 and c_0/b ratios became equal again due to formation of a triangular network of the Fe atoms and superstructure $\sqrt{3} \times \sqrt{3} \times 2$ (space group $P\bar{3}1c$) as shown on the left panel of Fig. 1 for $x = 0.33$. The monoclinic system and the difference between c_0/a_0 and c_0/b values appear in Fe_xTiS_2 with further growth of the Fe concentration above $x \sim 0.45$, where a monoclinic $\sqrt{3} \times 1 \times 2$ superstructure (space group $I12/m1$) is formed. The superstructure that forms at $x = 0.50$ is shown in the scheme in Fig. 1. With an increase in the iron content above $x = 0.50$, the vacant positions between the chains begin to be partially occupied.

$Fe_{0.25}TiS_2$. To clarify the magnetic state of the $Fe_{0.25}TiS_2$ compound and its intriguing magnetoresistance behavior, we performed neutron diffraction measurements in the temperature range 2–100 K, i.e., above and below the magnetic critical temperature $T_{ord} \approx 52$ K. This value was determined from the temperature dependencies of the magnetic susceptibility [Fig. 1(d)] and the electrical resistivity data [20,21] and agrees with the critical temperature reported by other authors [33,34]. Figure 2 shows the NPD patterns for $Fe_{0.25}TiS_2$ measured in the paramagnetic state at $T = 100$ K and in the magnetically ordered state at $T = 2$ K. From the NPD pattern at 100 K, the crystal structure of $Fe_{0.25}TiS_2$ can be described in the same space group $C12/m1$, which was determined from the room-temperature x-ray data for this compound [21,35]. Upon cooling below ∼60 K, new weak reflections were observed to appear in the NPD pattern, which could not be associated with nuclear Bragg scattering. Magnetic Bragg reflections are marked by arrows in Fig. 2(b). Figure 2(c) shows the evolution of the scattering intensity with temperature in the angle interval $10° < 2\theta < 22°$. The fact that the appearance of additional reflections correlates with an anomalous change in the
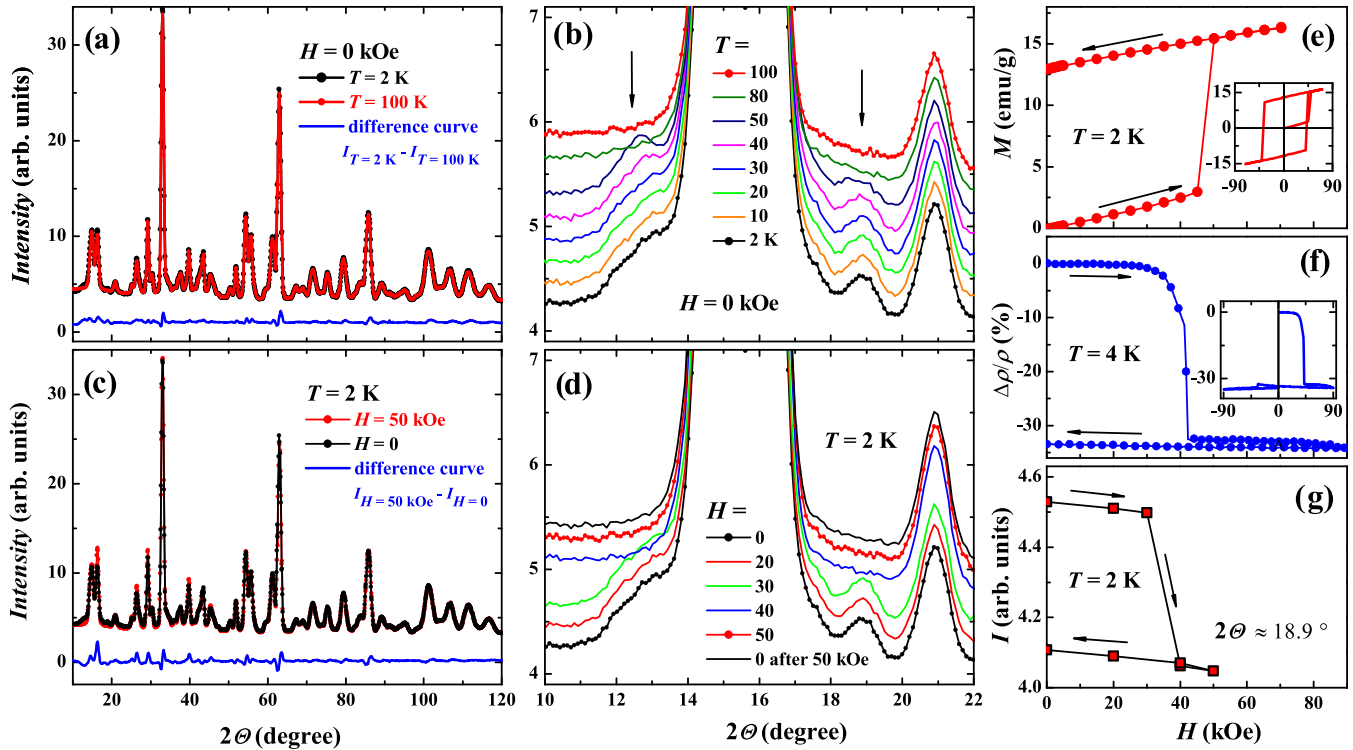
FIG. 2. (a) NPD patterns measured with neutron wavelength $\lambda = 1.5$ Å on the $Fe_{0.25}TiS_2$ sample at temperatures 100 K and 2 K in zero magnetic field; (b) temperature evolution of the NPD pattern in the range $10° \leqslant 2\theta \leqslant 22°$; (c) the magnetic field effects on the NPD patterns at $T = 2$ K; (d) the magnetic field effects on the NPD patterns at $T = 2$ K in the range $10° \leqslant 2\theta \leqslant 22°$. Right panel displays field dependencies of the magnetization at $T = 2$ K (e), magnetoresistance at $T = 4$ K (f), and intensity of the reflection around $2\theta \approx 18.9°$ at $T = 2$ K (g). Insets show the full magnetization and magnetoresistance loops.

magnetic susceptibility [Fig. 1(d)] indicates an antiferromagnetic order of the Fe magnetic moments in this compound with cooling. Note that the Fe-intercalated diselenide compound $Fe_{0.25}TiSe_2$ with the same Fe concentration was shown to exhibit an AFM order as well [36].

It is worth emphasizing here that the temperature dependence of the magnetic susceptibility of $Fe_{0.25}TiS_2$ measured in the field cooling (FC) regime [Fig. 1(c)] looks very unusual for AFM ordered materials and such behavior can rather be found in highly anisotropic ferromagnets with a large coercive force. Also, the wide, almost rectangular hysteresis loop observed in this sample at low temperatures is characteristic of a highly anisotropic ferromagnet. However, the presence of additional Bragg reflections in the NPD pattern for $Fe_{0.25}TiS_2$ and their field dependence leaves no doubt that the ground magnetic state of this compound is antiferromagnetic. As can be clearly seen in Fig. 2(d), which displays changes in the neutron scattering in the range $10° < 2\theta < 22°$, an increase in the magnetic field up to 40 kOe results in a sharp decrease in the intensity of the AFM reflections. After switching off the field, the intensities of these reflections do not return to their initial values, which indicates the formation of a metastable FM state. The initial AFM state in this compound can be achieved after heating the sample above the Néel temperature and subsequent cooling without a magnetic field. Figure 2(g) shows, as an example, the field dependence of the maximal intensity of the broad maxima around $2\theta \approx 18.9°$. There is an obvious correlation between the variations of the magnetic diffraction peaks [Fig. 2(g)] and magnetoresistance [Fig. 2(f)]

with the magnetic field. The obtained NPD data allow us to explain the observation of a large remnant magnetoresistance [Figs. 1(c) and 2(f)] in $Fe_{0.25}TiS_2$ in the following scenario. Because of the AFM ground state, the $Fe_{0.25}TiS_2$ compound exhibits an increased resistivity due to the formation of superzone gaps on the Fermi surface [22]. In $Fe_{0.25}TiS_2$, the field-induced phase transition from the AFM magnetic structure to the FM state is accompanied by the disappearance of superzones and energy gaps on superzone boundaries, which leads to a decrease in the resistivity. A further variation of the field in the metastable FM state does not lead to restoration of the initial AFM arrangement of the Fe magnetic moments and the resistivity as well. The fact that field-induced AFM-FM transitions in metallic antiferromagnets are accompanied by a rearrangement of the Fermi surface and a significant change not only in the electrical resistivity, but also in the electronic heat capacity, Hall effect, and thermoelectric power is confirmed by data obtained for some other materials with metallic conductivity and AFM ordering (see Refs. [37,38], for instance).

It should be noted that Kuroiwa *et al.* [39] do not find any magnetic Bragg reflections in the neutron diffraction measurements of the $Fe_{0.25}TiS_2$. This discrepancy in the NPD data for this compound can be associated with a different degree of order in the subsystem of intercalated Fe atoms due to the difference in sample preparation. Changes in the distribution of Fe atoms and vacancies caused by heat treatments of the $Fe_{0.25}TiS_2$ samples under different conditions are found to significantly affect the MR response and the volume of the
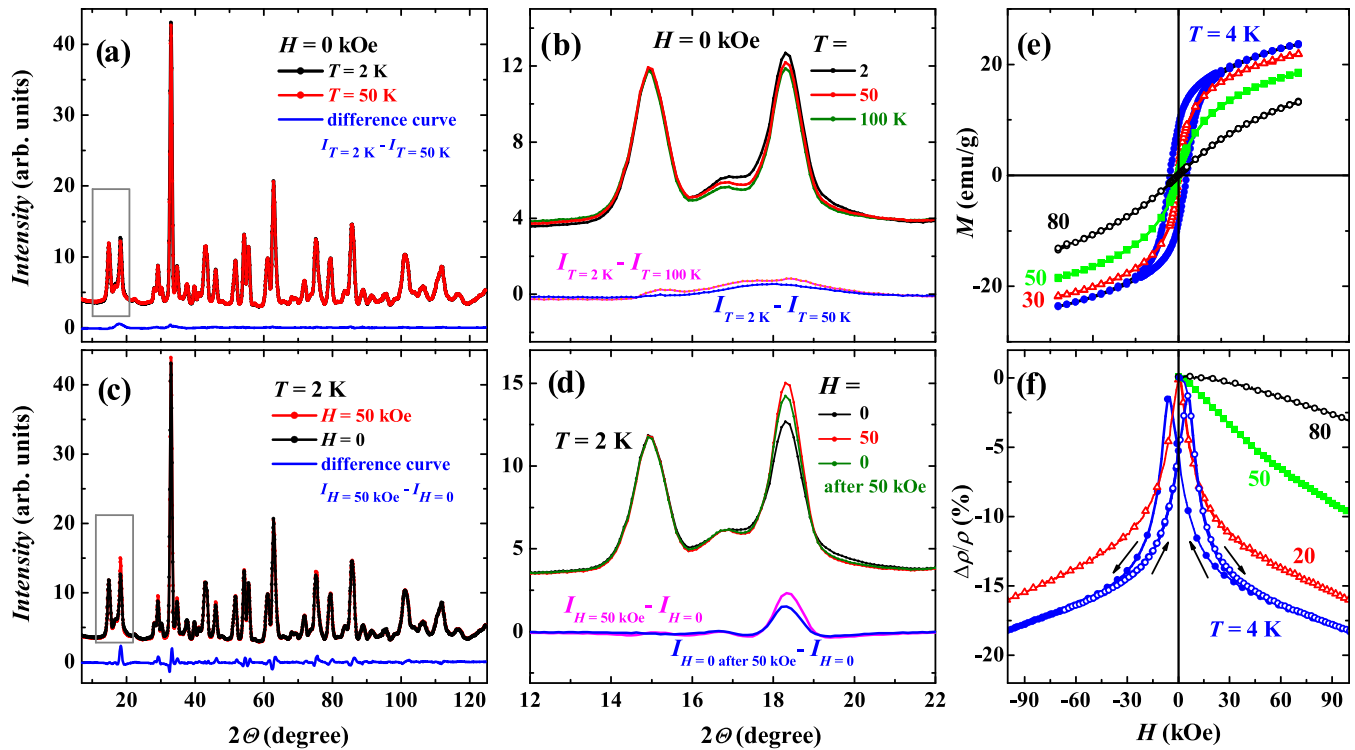
FIG. 3. (a) NPD patterns for the $Fe_{0.33}TiS_2$ sample measured with neutron wavelength $\lambda = 1.5$ Å at various temperatures; (b) temperature evolution of the NPD pattern in the range $12° \leqslant 2\theta \leqslant 22°$; (c) the magnetic field effects on the NPD patterns at $T = 2$ K; (d) the effect of a magnetic field on neutron scattering at 2 K in the range $12° \leqslant 2\theta \leqslant 22°$. Difference curves are shown at the bottom. Right panel displays field dependencies of the magnetization (e) and magnetoresistance (f) at various temperatures.

AFM phase experiencing a field-induced phase transition to the FM state, as shown in Appendix.

$Fe_{0.33}TiS_2$. Figure 3 shows the NPD data obtained for the $Fe_{0.33}TiS_2$ sample at various temperatures and magnetic fields together with field dependencies of the magnetization and magnetoresistance. All nuclear peaks on the NPD pattern at temperature 100 K are indexed within the space group $P\bar{3}1c$ used to describe the room-temperature x-ray data. In contrast to the $Fe_{0.25}TiS_2$, neutron diffraction measurements on the $Fe_{0.33}TiS_2$ sample at $T = 2$ K did not reveal any additional reflections and substantial changes in the intensity of Bragg nuclear peaks compared to the NPD patterns obtained in the paramagnetic state (at 50 K and 100 K). These data support the earlier assumption that there is no long-range magnetic order in this compound [20,39]. As follows from Fig. 3(c), only broad diffuse maximum in the range $15° \leqslant 2\theta \leqslant 21°$ is seen on difference intensity plot. The fact that there is no periodic arrangement of the Fe spins in $Fe_{0.33}TiS_2$ may be attributed to the frustrations of exchange interactions of different signs [40] between Fe spins due to the formation of a triangular network in the ab plane (Fig. 1, left panel). The absence of a long-range magnetic order in this compound derived from neutron diffraction data is consistent with smooth changes in the magnetization and a reduced coercivity compared to the $M(H)$ curves for $Fe_{0.25}TiS_2$ [Fig. 2(e)].

The cluster glass magnetic state arises in $Fe_{0.33}TiS_2$ with decreasing temperature below the freezing temperature $T_f \approx 44$ K [Fig. 1(e)]. As can be seen from Figs. 3(b) and 3(d), application of the 50 kOe magnetic field at $T = 2$ K leads to the suppression of the diffuse magnetic scattering and

growth of the magnetic contribution to the Bragg peaks. Such changes in the neutron scattering mean that the application of a magnetic field leads to the transformation of the cluster-glass magnetic state towards ferromagnetic alignment of the Fe magnetic moments in $Fe_{0.33}TiS_2$. It is interesting to note that the neutron scattering intensities on the $Fe_{0.33}TiS_2$ sample do not reinstate to their initial values after switching off the field [Fig. 3(d)]. The isothermal field dependencies of the magnetization [Fig. 3(e)] and MR [Fig. 3(f)] observed for $Fe_{0.33}TiS_2$ below T_f turned out to be quite typical for cluster glass materials. The MR isotherm measured at 5 K shows hysteresis which reflects the change in the magnetization.

In this sample, the applied magnetic field apparently rotates the magnetic moments of clusters toward the field direction, which is accompanied by a gradual reduction of the resistivity by about 18% in a magnetic field $\sim$100 kOe. After zeroing the magnetic field, the electrical resistivity of this compound is found to be lower (by $\sim$5%) than the initial value. This type of magnetoresistance behavior is characteristic for magnetically inhomogeneous cluster-glass or granular systems [41]. A small remnant magnetoresistance is indicative of changes in the arrangement of the Fe magnetic moments in clusters induced by the applied field, which is consistent with irreversibilities observed in neutron scattering [Fig. 3(d)]. As the temperature rises, the expected decrease in magnetic hysteresis and MR occurs.

$Fe_{0.50}TiS_2$. An increase in the Fe content in Fe_xTiS_2 up to $x = 0.50$ dramatically affects the magnetic state and magnetoresistance behavior. According to the Rietveld refinement of the NPD pattern measured with neutron wavelength
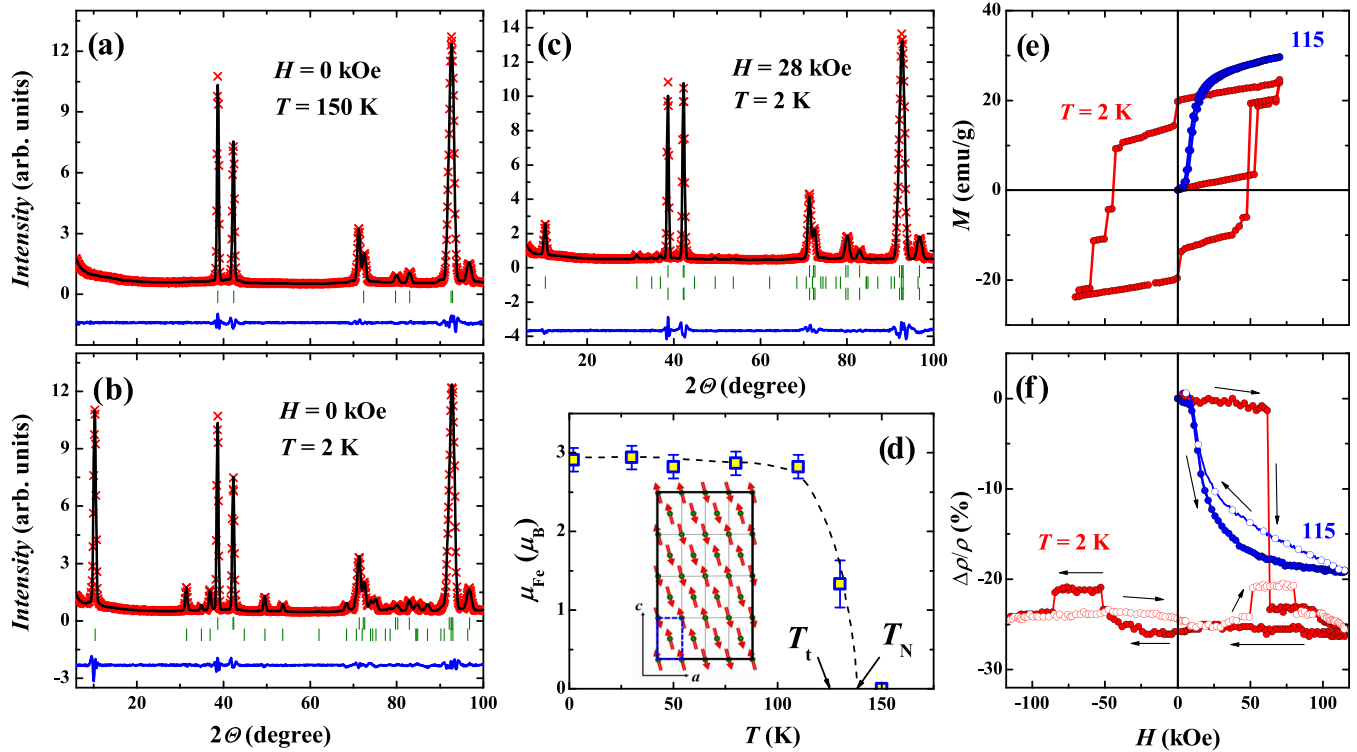
FIG. 4. NPD pattern for $Fe_{0.50}TiS_2$ measured with neutron wavelength $\lambda = 3.8$ Å in zero field on the ZFC sample at 150 K (a) and 2 K (b), and on the sample cooled at the 28 kOe field down to 2 K (c). The red symbols represent the experimental profile and the solid black line represents the results of the fit using the Rietveld refinement. The upper row of vertical marks indicates the positions of nuclear Bragg reflections, second row the position of Bragg peaks corresponding to the AFM structure with the propagation vector $\mathbf{k} = [\frac{1}{4}\ 0\ \frac{1}{4}]$, and third row the positions of Bragg reflections corresponding to the field-induced FM state. (d) The temperature variation of the magnetic moment of Fe obtained from the Rietveld refinement of the NPD patterns measured at various temperatures. The dashed line is drawn by eye. Inset shows the scheme of the arrangement of the Fe magnetic moments in the *ac* crystallographic plane; the crystallographic cell is indicated by dashed line (titanium and sulfur atoms omitted for clarity). Right panel shows field dependencies of the magnetization at 2 K (e) and magnetoresistance at 4 K (f).

$\lambda = 3.8$ Å at the DMC diffractometer (SINQ, Switzerland) in the paramagnetic state at 150 K [Fig. 4(a)] the nuclear Bragg reflections can be well described by the model with a monoclinic crystal structure (space group $I12/m1$) derived from the x-ray diffraction study [18]. The best fit result ($R_B = 1.62\%$) for data at 150 K is obtained for the composition $Fe_{0.492}TiS_2$, which is close to the nominal one. This compound undergoes a transition from the paramagnetic state to the AFM order upon cooling below $T_N \approx 140$ K, which manifests itself in the appearance of additional reflections in the NPD pattern. However, it was found that the NPD pattern measured below T_N on a Fe_xTiS_2 sample depends significantly on the cooling regime. As is shown in Fig. 4(b), a set of the AFM reflections is clearly visible in the NPD pattern measured in zero field at $T = 2$ K on the ZFC sample, while these AFM peaks turned out to be substantially reduced when the sample was cooled in a field of 28 kOe [Fig. 4(c)]. In addition, cooling in the 28 kOe field resulted in an additional FM contribution to the intensity of the nuclear Bragg peaks. The magnetic structure of the ZFC sample at 2 K can be well described with $R_{mag} = 6.9\%$ by the wave vector $\mathbf{k} = [\frac{1}{4}, 0, \frac{1}{4}]$. The magnetic moments of iron $\mu_{Fe} \sim 2.9\mu_B$ lie in the *ac* plane and deviate from the *c* axis by an angle of about 11.4°. This magnetic structure is quadrupled in the *a* and *b* direction of the crystallographic axes, as shown in Fig. 4(e). These data are consistent with

previous studies [18,42]. Our value of μ_{Fe} is quite close to a value obtained from analysis of the XMCD spectra for the sample with composition close to $Fe_{0.50}TiS_2$ [27]. According to x-ray absorption spectroscopy and x-ray magnetic circular dichroism measurements iron atoms in $Fe_{0.50}TiS_2$ are fully in the valence states of 2+ and exhibit a spin magnetic moment $\sim 2.5\mu_B$ and orbital magnetic moment $\sim 0.6\mu_B$ [27]. A reduced value of spin magnetic moment in $Fe_{0.50}TiS_2$ in comparison with the Fe^{2+} ionic spin moment ($4\mu_B$) may be associated with the hybridization of 3*d* electrons of intercalated Fe ions with the Ti 3*d* states and S 3*p* states of the TiS_2 matrix. Temperature variation of the μ_{Fe} value determined from the Rietveld refinement of the NPD patterns measured at various temperatures is displayed in Fig. 4(e) as well. As can be seen, μ_{Fe} slightly decreases as the temperature rises to 110 K, and then drops with increasing temperature up to $T_N \approx 140$ K. It should be noted that according to a previous study [42] the magnetic structure between $T_t \approx 125$ K and T_N is incommensurate, and becomes commensurate with the crystal lattice when cooled below 125 K. The magnetic state of the $Fe_{0.50}TiS_2$ sample at $T = 2$ K after cooling at $H = 28$ kOe from 160 K is characterized as heterogeneous. The magnetic heterogeneity obviously results from the poly-crystallinity of the sample; therefore, upon cooling in the field, not all particles turned out to be in a ferromagnetic state due
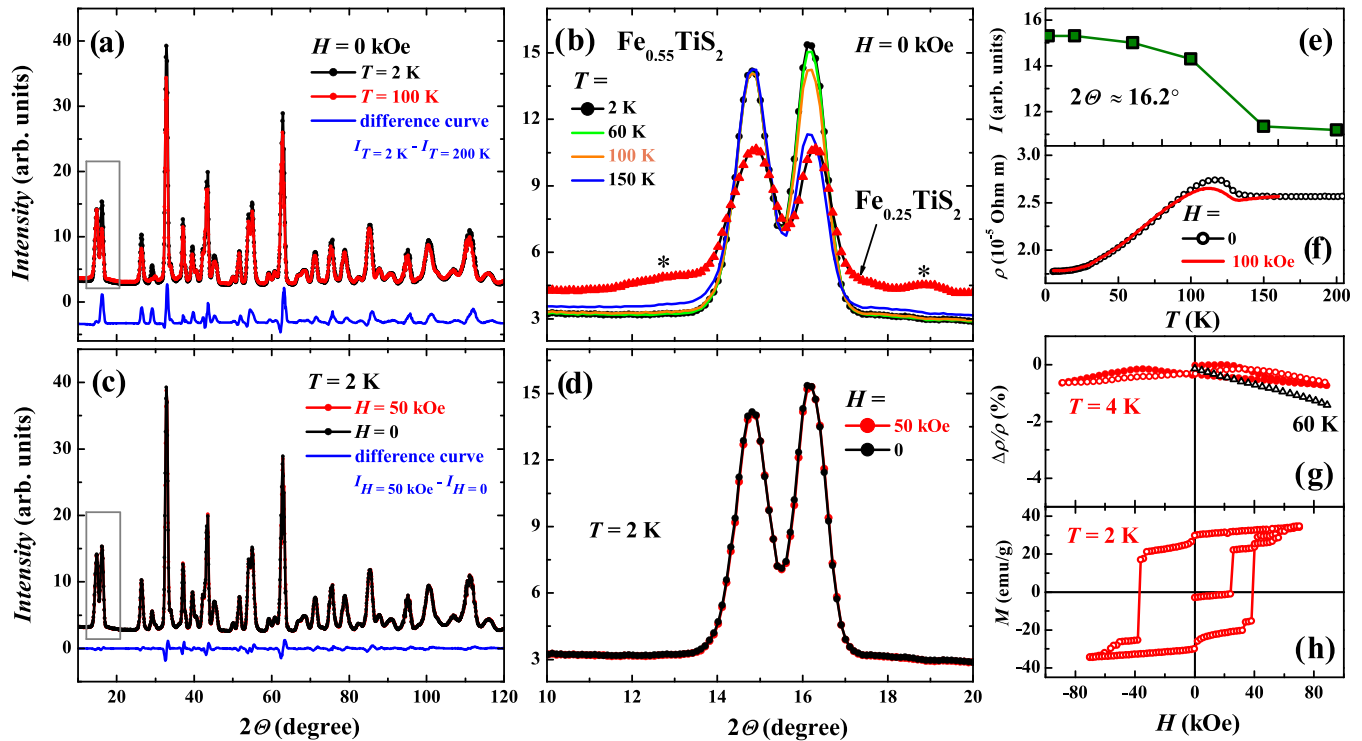
FIG. 5. (a) NPD patterns for the $Fe_{0.55}TiS_2$ sample measured with neutron wavelength $\lambda = 1.5$ Å at 2 K and 100 K; (b) temperature evolution of the NPD pattern for $Fe_{0.55}TiS_2$ in the range $10° \leqslant 2\theta \leqslant 20°$ and the part of the NPD pattern for $Fe_{0.25}TiS_2$ at $T = 2$ K (stars indicate the AFM reflections). (c) The magnetic field effects on the NPD patterns at $T = 2$ K; (d) influence of the magnetic field on neutron scattering at 2 K in the range $12° \leqslant 2\theta \leqslant 22°$. Difference curves are shown at the bottom. Right panel shows temperature dependencies of the intensity of the reflection at $2\theta \sim 16.2°$ (e), electrical resistivity at $H = 0$ (symbols) and at $H = 100$ kOe (line) for $Fe_{0.55}TiS_2$ (f), and field dependencies of the magnetoresistance (g) and magnetization (h) for $Fe_{0.55}TiS_2$.

to the high magnetocrystalline anisotropy. The refinement of the NPD pattern displayed in Fig. 4(c) has shown that best fit result can be obtained in a model that takes into account the presence of about 20% of the AFM phase along with the field-induced FM phase. These NPD data allowed us to explain the unusual behavior of the magnetoresistance at low temperatures [Fig. 4(f)], despite the observation of an FM-like hysteresis loop in this compound at low temperatures [Fig. 4(e)]. As is seen, the application of an external magnetic field above a critical value H_c results in step-like jumps of both the magnetization and magnetoresistance, which corresponds to the metamagnetic transition from AFM to the induced FM state in $Fe_{0.50}TiS_2$. The further field cycling keeps this sample in the metastable FM state which can be observed in this compound at temperatures up to ≈ 70 K. The metastable FM state can be detected by the observation of the remnant MR. The mean-field analysis performed for an AFM system with intralayer and interlayer exchange interactions between the Ising spins has shown that the magnetoelastic coupling can be responsible for the presence of the metastable field-induced FM state [19]. As the temperature rises above 70 K, thermal fluctuations destroy the metastable FM state in $Fe_{0.50}TiS_2$ and the behavior of the magnetization in this compound becomes typical of antiferromagnets undergoing a metamagnetic transition. As can be seen from Fig. 4(e), the field dependence of the magnetization at 115 K has a shape typical of metamagnets with a sharp growth of the magnetization with the increasing field above the critical value of about 6 kOe and

with a tendency to saturation with a further increase in the field. The magnetoresistance measured at 115 K shows a sharp decrease in almost the same field and shows no remnant value in contrast to low low-temperature behavior. Since, according to neutron diffraction data, the field-induced AFM-FM transition in the polycrystalline $Fe_{0.50}TiS_2$ sample does not occur in the entire volume of the sample [see Fig. 4(c)] it can be expected that a single-crystalline sample will have a higher MR value.

$Fe_{0.55}TiS_2$. Figure 5 shows the results of the NPD measurements along with the results of magnetization and magnetoresistance studies for $Fe_{0.55}TiS_2$. In contrast to $Fe_{0.50}TiS_2$, the NPD pattern obtained for this compound at 150 K, i.e., above magnetic critical temperature ~ 141 K [Fig. 1(f)], can be described by the model of a monoclinic crystal structure (space group $C12/m1$) suggested for $Fe_{0.25}TiS_2$ exhibiting $2\sqrt{3} \times 2 \times 2$ superstructure with enlarged unit cell dimensions in comparison with the $\sqrt{3} \times 1 \times 2$ superstructure observed in $Fe_{0.50}TiS_2$. It seems that an increase in the Fe content above $x = 0.5$ leads to disruption of the ordered arrangement of iron atoms in neighboring octahedral sites in the layer, which was observed at $x = 0.50$ (Fig. 1, left panel). Taking into account the fact that the energies of the AFM and FM states in this system differ insignificantly, such changes in the distribution of Fe atoms should lead to a transformation of the magnetic structure. Indeed, as follows from the NPD measurements [see Figs. 5(a) and 5(b)], the appearance of a magnetic order upon cooling to 2 K did not lead to the appearance of

additional reflections, the angular position of which differs from the position of the nuclear Bragg reflections. We added in Fig. 5(b) a part of the NDP pattern at $T = 2$ K for $Fe_{0.25}TiS_2$ for comparison, where the AFM reflections are marked with stars. When we compare the intensities of neutron scattering on the $Fe_{0.55}TiS_2$ sample at 150 K and 2 K [Figs. 5(a) and 5(b)], it can be seen that, in the magnetically ordered state, there is a noticeable magnetic contribution to the intensity of the Bragg peaks. The temperature dependence of the intensity of the peak at $2\theta \sim 16.2°$ is shown as an example in Fig. 5(e). It can be seen that the intensity of the magnetic contribution disappears as the critical temperature is approached. From the absence of additional magnetic peaks on the NPD patterns below magnetic critical temperature, we may conclude that the magnetic structure of $Fe_{0.55}TiS_2$ is commensurate with the crystal lattice and it is described by the propagation vector $\mathbf{k} = [0, 0, 0]$.

To reveal the influence of the magnetic field on the magnetic state of $Fe_{0.55}TiS_2$, we have performed the NPD measurements in an applied field of 50 kOe. As follows from Figs. 5(c) and 5(d), which display both the zero-field NPD pattern and the pattern measured at $H = 50$ kOe, the influence of the 50 kOe magnetic field on the neutron scattering is rather small compared to other Fe_xTiS_2 compounds with lower Fe concentrations [see Figs. 2(f), 3(f), and 4(f)], although it can be seen that the application of the 50 kOe field still causes a slight increase in the intensity of the Bragg reflections. In contrast to the compounds with the AFM virgin state, the $Fe_{0.55}TiS_2$ compound does not exhibit remarkable changes in the electrical resistivity under application of the magnetic field. Low impact of the magnetic field on the transport properties of $Fe_{0.55}TiS_2$ demonstrates the temperature dependence of the electrical resistivity measured without field and in an applied field of 100 kOe. As follows from Fig. 5(f), a difference between the zero-field resistivity and resistivity measured at $H = 100$ kOe becomes noticeable only in the vicinity of the magnetic critical temperature, while at low temperatures, $| \Delta\rho/\rho |$ is rather small and varies within $0 - 1.0\%$ [Fig. 5(g)].

As to the magnetization behavior, the $Fe_{0.55}TiS_2$ compound exhibits a broad hysteresis loop Fig. 5(h) with the coercive field of about 40 kOe, which is comparable with H_c values observed in the field-induced metastable FM states in $Fe_{0.25}TiS_2$ [Fig. 2(e)] and $Fe_{0.5}TiS_2$ [Fig. 4(e)]. All these data allow us to suggest that $Fe_{0.55}TiS_2$ exhibits ferromagnetic or ferrimagnetic order. Based on the analysis of the behavior of the magnetization, the existence of a ferrimagnetic ordering of the Fe magnetic moments was also assumed earlier in the $Fe_{0.66}TiS_2$ [43] compound with a higher Fe content. According to the neutron diffraction data available in the literature [18,31,36,39,42,44], the Fe atoms in Fe_xTiX_2 compounds (X = S, Se) in which the Fe content does not exceed $x = 0.50$ are predominantly located in the layer between X-Ti-X sandwiches. However, it should be mentioned that, according to neutron diffraction studies of the selenide compounds Fe_xTiSe_2 [36], the best agreement between the observed and calculated intensities is achieved if about 8% of metal sites in an Fe layer are occupied by Ti atoms and consequently some Ti atoms in a Ti layer are substituted by Fe atoms. The partial mixing of Ti and Fe atoms was revealed

by NPD measurements in the sulfide compound $Fe_4Ti_3S_8$ ($FeTi_{0.75}S_2$) with a layered crystal structure of the NiAs-type and ferrimagnetic order [45].

The incomplete cation partitioning was also detected by neutron diffraction in the Fe-containing compounds $Fe_xV_{3-x}S_4$ [46]. It should be emphasized here that, according to neutron diffraction and magnetization studies [18,36,42,45,47], most other iron-bearing sulfides and selenides with a layered NiAs-type crystal structure exhibit AFM or ferrimagnetic order due to AFM coupling between adjacent cationic layers. An exception are the Fe_xTaS_2 compounds based on tantalum disulfide, which exhibit ferromagnetic order [48,49]. Therefore, the ferrimagnetic order in Fe_xTiS_2 compounds with $x > 0.50$ may result from the AFM coupling of the Fe magnetic moments located in alternating layers with different Fe occupation.

IV. SUMMARY AND CONCLUSION

For a deeper understanding of the mechanisms that determine the behavior of magnetoresistance in intercalated transition metal dichalcogenides, in this work, we have performed a comprehensive study of Fe_xTiS_2 compounds with various Fe concentrations in the range of $0.25 \leqslant x \leqslant 0.55$ using magnetization and magnetoresistance measurements, as well as the neutron powder diffraction studies in magnetic fields up to 50 kOe at temperatures from 2 K to 200 K. Polycrystalline samples for this study were synthesized by the method of solid-state reactions with long-term (up to four weeks) homogenizing heat treatment. According to our NPD data collected in the paramagnetic region, the crystal structure of these compounds changes with the concentration of Fe, as was previously shown by x-ray diffraction. Starting from $x = 0.25$, various orderings of Fe atoms were revealed in this system with increasing x, which result in the observed changes in the magnetic state. The latter, in turn, manifests itself in dramatic changes in the behavior of the magnetoresistance. In contrast to the cluster-glass magnetic state associated with the disorder in the subsystem of Fe atoms in compounds with $x < 0.25$, the order of Fe atoms and formation of a monoclinic superstructure in $Fe_{0.25}TiS_2$ results in the appearance of an AFM order below the Néel temperature $T_N \approx 52$ K, as evidenced by neutron diffraction measurements.

As follows from the NPD data, the application of a magnetic field leads to irreversible suppression of AFM reflections, which indicates the occurrence of a field-induced phase transition from the AFM to the metastable FM state. A similar scenario in the behavior of magnetization and neutron scattering upon application of a magnetic field plays out in the $Fe_{0.50}TiS_2$ compound with a monoclinic superstructure and AFM virgin state. In both of these antiferromagnetically ordered compounds, the AFM to FM transition is accompanied by largely irreversible changes in the magnetoresistance due to the superzone effect [22]

The formation of the metastable FM state at low temperatures in the compounds with $x = 0.25$ and $x = 0.50$ is characterized by the presence of the giant remnant magnetoresistance ($| \Delta\rho_{rem}/\rho | \sim 25$–35%). The irreversibility of the AFM-FM transition in Fe_xTiS_2 with $x \approx 0.25$ and $x \approx 0.50$ is suggested to result from the Ising character of Fe ions

together with magnetoelastic interaction [19]. Note that the formation of the metastable FM state was observed in some other antiferromagnetically ordered compounds with a high magnetocrystalline anisotropy [50–53]. The low-temperature values of the coercive field in Fe_xTiS_2 are found to vary nonmonotonically within the range ~10–55 kOe [20,54]. The maximal values of H_c are observed in compounds exhibiting the AFM state, i.e., with Fe concentrations $x \sim 0.25$ and $x \sim 0.50$, which implies that such an enhancement of the coercivity may be influenced not only by the presence of a large orbital moment of Fe [26,27], but also by the intrinsic exchange bias [55].

The $Fe_{0.33}TiS_2$ compound located on the concentration scale between two antiferromagnetically ordered compounds with $x = 0.25$ and $x = 0.50$ is found to possess abnormal properties. Instead of the jump-like and irreversible changes in magnetization and magnetoresistance associated with field-induced AFM-FM transition, the $Fe_{0.33}TiS_2$ compound shows temperature and field dependencies of the magnetization characteristic of cluster spin glasses. The MR behavior in this compound is observed to be quite usual for cluster glasses as well. According to neutron diffraction studies, the $Fe_{0.33}TiS_2$ compound does not have a long-range magnetic order. An applied magnetic field is found to suppress the diffuse magnetic scattering associated with short-range magnetic correlations in $Fe_{0.33}TiS_2$ and leads to an increase in the magnetic contribution to the Bragg peaks. The absence of a long-range magnetic order at $x = 0.33$ is attributed to the formation of a triangular network of Fe atoms in the *ab* plane and the frustrations of exchange interactions.

In contrast to $Fe_{0.50}TiS_2$ with a low-temperature AFM structure [18,42], the magnetic unit cell of the $Fe_{0.55}TiS_2$ compound with a slightly higher Fe content is observed to coincide with the crystal unit cell and the propagation vector of the magnetic structure for $Fe_{0.55}TiS_2$ is $\mathbf{k} = [0, 0, 0]$. Low magnetoresistance values in this compound ($| \Delta\rho_{rem}/\rho | \sim 1\%$) at low temperatures (~4 K) are attributed to the ferromagnetic or ferrimagnetic order of the Fe magnetic moments. Ferrimagnetic ordering can arise due to the possible mixing of Ti and Fe atoms and AFM interactions between the iron atoms located in neighbor cationic layers. However, to confirm this assumption, further high-resolution neutron diffraction studies of the distribution of Fe and Ti atoms inside and between cationic layers in Fe_xTiS_2 with $x > 0.50$ would be desirable.

In conclusion, using the Fe_xTiS_2 as a unique example, we present a study of the effect of magnetic order on the magnetoresistance behavior in the intercalated layered system. We show that the magnetic state and the corresponding behavior of the magnetoresistance are determined primarily by the distribution of the intercalated atoms both inside and between the cationic layers. Our results would help to understand the behavior of magnetoresistance in other layered systems and find ways to tune the structure of materials for their efficient applications.
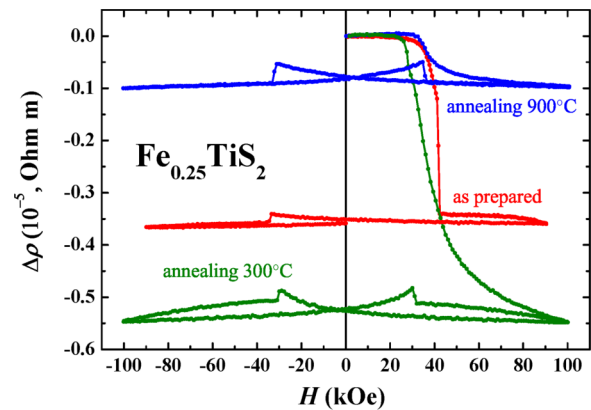
ACKNOWLEDGMENTS

FIG. 6. The change in electrical resistivity $\Delta\rho = [\rho(H) - \rho(0)]$ at 4 K as a function of the magnetic field for a $Fe_{0.25}TiS_2$ sample after heat treatment at various temperatures.

APPENDIX: ANNEALING EFFECT

In order to reveal whether the degree of ordering of the intercalated Fe atoms affects the change in resistivity during the AFM–FM transition, various heat treatments of the $Fe_{0.25}TiS_2$ sample were carried out. Figure 6 shows the field dependencies of the change in the electrical resistivity $\Delta\rho$ of the $Fe_{0.25}TiS_2$ sample after three weeks of annealing at 300 °C and after annealing at 900 °C for 4 days. The data for the as-prepared sample are also presented for comparison. In all cases, the samples were cooled by removing the ampule from the furnace into the air. As can be seen from Fig. 6, a sharp drop of the resistivity is observed in the samples with increasing field above a critical value, which is associated with the phase transition from the initial AFM to the metastable FM state. However, the change in the electrical resistivity of the samples $\Delta\rho_{AFM-FM}$ in high magnetic fields (90–100 kOe) is found to be different for different heat treatment conditions. As for the as prepared sample, the large remnant magnetoresistance after switching off the field is also observed for the samples annealed at 900 °C and 300 °C. Absolute value of $| \Delta\rho_{AFM-FM} |$ turned out to be higher for the sample after 300 °C heat treatment and lower after heat treatment at 900 °C compared to the as-prepared sample. Such a difference in $| \Delta\rho_{AFM-FM} |$ values implies the formation of inhomogeneous magnetic states in samples with different volumes of the AFM phase since $| \Delta\rho_{AFM-FM} |$ is proportional to the volume of the AFM phase which can transform into the FM state under the application of a magnetic field. Taking into account the analysis of the electrical resistivity of the two-phase composite [56], the lower value of $|\Delta\rho_{AFM-FM}|$ observed in $Fe_{0.25}TiS_2$ after heat treatment at 900 °C can be explained by the disorder of the Fe atoms and vacancies located between the S-Ti-S sandwiches and the formation of the AFM order at low temperatures in a relatively small volume of the sample. However, after heat treatment at 300 °C, the volume fraction of the AFM phase is approximately three times higher. Note that deviation of the Fe content from $x = 0.25$ also leads to the heterogeneous magnetic state with coexisting AFM and CG phases [20].

[1] S. Manzeli, D. Ovchinnikov, D. Pasquier, O. V. Yazyev, and A. Kis, 2D transition metal dichalcogenides, Nat. Rev. Mater. **2**, 17033 (2017).

[2] G. H. Han, D. L. Duong, D. H. Keum, S. J. Yun, and Y. H. Lee, van der Waals metallic transition metal dichalcogenides, Chem. Rev. **118**, 6297 (2018).

[3] J. Shi, M. Hong, Z. Zhang, Q. Ji, and Y Zhang, Physical properties and potential applications of two-dimensional metallic transition metal dichalcogenides, Coord. Chem. Rev. **376**, 1 (2018).

[4] P. Zhao, J. Li, H. Jin, L. Yu, B. Huang, and D. Ying, Designing lateral spintronic devices with giant tunnel magnetoresistance and perfect spin injection efficiency based on transition metal dichalcogenides, Phys. Chem. Chem. Phys. **20**, 10286 (2018).

[5] B. Zhao, D. Shen, Z. Zhang, P. Lu, M. Hossain, J. Li, B. Li, and X. Duan, 2D Metallic Transition–Metal Dichalcogenides: Structures, Synthesis, Properties, and Applications, Adv. Funct. Mater. **31**, 2105132 (2021).

[6] A. Y. Ledneva, G. E. Chebanova, S. B. Artemkina, and A. N. Lavrov, Crystalline and nanostructured materials based on transition metal dichalcogenides: synthesis and electronic properties, J. Struct. Chem. **63**, 176 (2022).

[7] A. H. Castro Neto, Charge Density Wave, Superconductivity, and Anomalous Metallic Behavior in 2D Transition Metal Dichalcogenides, Phys. Rev. Lett. **86**, 4382 (2001).

[8] Z. Xu, H. Yang, X. Song, Y. Chen, H. Yang, M. Liu, Z. Huang, Q. Zhang, J. Sun, L. Liu, and Y. Wang, Topical review: Recent progress of charge density waves in 2D transition metal dichalcogenide-based heterojunctions and their applications, Nanotechnology **32**, 492001 (2021).

[9] Z. Wang, R. Li, C. Su, and K. P. Loh, Intercalated phases of transition metal dichalcogenides, SmartMat. **1**, e1013 (2020).

[10] M. N. Ali, J. Xiong, S. Flynn, J. Tao, Q. D. Gibson, L. M. Schoop, T. Liang, N Haldolaarachchige, M. Hirschberger, N. P. Ong, R. J. Cava, Large, non-saturating magnetoresistance in WTe$_2$, Nature (London) **514**, 205 (2014).

[11] P. K. Das, D. Di Sante, F. Cilento, C. Bigi, D. Kopic, D. Soranzio, A. Sterzi, J. A. Krieger, I. Vobornik, J. Fujii, T. Okuda, V. N. Strocov, M. B. H. Breese, F. Parmigiani, G. Rossi, S. Picozzi, R. Thomale, G. Sangiovanni, R. J. Cava, and G. Panaccione, Electronic properties of candidate type-II Weyl semimetal WTe$_2$. A review perspective, Electron. Struct. **1**, 014003 (2019).

[12] S. Mangelsen, P. G. Naumov, O. I. Barkalov, S. A. Medvedev, W. Schnelle, M. Bobnar, S. Mankovsky, S. Polesya, C. Näther, H. Ebert, and W. Bensch, Large nonsaturating magnetoresistance and pressure-induced phase transition in the layered semimetal HfTe$_2$, Phys. Rev. B **96**, 205148 (2017).

[13] Q. Zhou, D. Rhodes, Q. R. Zhang, S. Tang, R. Schönemann, and L. Balicas, Hall effect within the colossal magnetoresistive semimetallic state of MoTe$_2$, Phys. Rev. B **94**, 121101(R) (2016).

[14] J. Smit, Magnetoresistance of ferromagnetic metals and alloys at low temperatures, Physica **17**, 612 (1951).

[15] T. McGuire, and R. L. Potter, Anisotropic magnetoresistance in ferromagnetic 3d alloys, IEEE Trans. Magn. **11**, 1018 (1975).

[16] W. J. Hardy, C.-W. Chen, A. Marcinkova, H. Ji, J. Sinova, D. Natelson, and E. Morosan, Very large magnetoresistance in Fe$_{0.28}$TaS$_2$ single crystals, Phys. Rev. B **91**, 054426 (2015).

[17] C.-W. Chen, S. Chikara, V. S. Zapf, and E. Morosan, Correlations of crystallographic defects and anisotropy with magnetotransport properties in Fe$_x$TaS$_2$ single crystals (0.23 $\leqslant$ $x \leqslant$ 0.35), Phys. Rev. B **94**, 054406 (2016).

[18] N. V. Baranov, E. M. Sherokalova, N. V. Selezneva, A. V. Proshkin, L. Keller, A. S. Volegov, and E. P. Proskurina, Magnetic order, field induced phase transition and magnetoresistance in the intercalated compound Fe$_{0.5}$TiS$_2$, J. Phys.: Condens. Matter **25**, 066004 (2013).

[19] N. V. Baranov, N. V. Selezneva, E. M. Sherokalova, Y. A. Baglaeva, A. S. Ovchinnikov, A. A. Tereshchenko, D. I. Gorbunov, A. S. Volegov, and A. A. Sherstobitov, Magnetic phase transitions, metastable states, and magnetic hysteresis in the antiferromagnetic compounds Fe$_{0.5}$TiS$_{2-y}$Se$_y$, Phys. Rev. B **100**, 024430 (2019).

[20] N. V. Selezneva, N. V. Baranov, E. M. Sherokalova, A. S. Volegov, and A. A. Sherstobitov, Multiple magnetic states and irreversibilities in the Fe$_x$TiS$_2$ system, Phys. Rev. B **104**, 064411 (2021).

[21] N. V. Selezneva, N. V. Baranov, E. M. Sherokalova, A. S. Volegov, and A. A. Sherstobitov, Remnant magnetoresistance and virgin magnetic state in Fe$_{0.25}$TiS$_2$, J. Magn. Magn. Mater. **519**, 167480 (2021).

[22] R. J. Elliott and F. A. Wedgwood, Theory of the resistance of the rare earth metals, Proc. Phys. Soc. London **81**, 846 (1963).

[23] J. Choe, K. Lee, C. L. Huang, N. Trivedi, and E. Morosan, Magnetotransport in Fe-intercalated TS$_2$: Comparison between $T = $ Ti and Ta, Phys. Rev. B **99**, 064420 (2019).

[24] T. Satoh, Y. Tazuke, T. Miyadai, and K. Hoshi, Ferromagnetic and reentrant spin glass properties in an Ising magnet Fe$_x$TiS$_2$, J. Phys. Soc. Jpn. **57**, 1743 (1988).

[25] F. Matsukura, Y. Tazuke, and T. Miyadai, ac-susceptibility study of Ising spin glasses: Fe$_x$TiS$_2$, J. Phys. Soc. Jpn. **58**, 3355 (1989).

[26] A. Yamasaki, S. Imada, A. Sekiyama, S. Suga, T. Matsushita, T. Muro, Y. Saitoh, H. Negishi, and M. Sasaki, Angle-resolved photoemission spectroscopy and magnetic circular dichroism in Fe-intercalated TiS$_2$, Surf. Rev. Lett. **09**, 961 (2002).

[27] G. Shibata, C. Won, J. Kim, Y. Nonaka, K. Ikeda, Y. Wan, M. Suzuki, T. Koide, A. Tanaka, S.-W. Cheong, and A. Fujimori, Large Orbital Magnetic Moment and Strong Perpendicular Magnetic Anisotropy in Heavily Intercalated Fe$_x$TiS$_2$, J. Phys. Chem. C **125**, 12929 (2021).

[28] M. Inoue, H. P. Hughes, and A. D. Yoffe, The electronic and magnetic properties of the 3d transition metal intercalates of TiS$_2$, Adv. Phys. **38**, 565 (1989).

[29] M. D. Frontzek, R. Whitfield, K. M. Andrews, A. B. Jones, M. Bobrek, K. Vodopivec, B. C. Chakoumakos, and J. A. Fernandez-Baca, WAND^2 - A versatile wide angle neutron powder/single crystal diffractometer, Rev. Sci. Instrum. **89**, 092801 (2018).

[30] J. Rodríguez-Carvajal, Recent advances in magnetic structure determination by neutron powder diffraction, Phys. B: Condens. Matter **192**, 55 (1993).

[31] Y. Kuroiwa, M. Nishimura, Y. Noda, and Y. Morii, Neutron powder diffraction study of intercalation compound Fe$_x$TiS$_2$, Phys. B: Condens. Matter **213–214**, 396 (1995).

[32] Y. L. Chiew, M. Miyata, M. Koyano, and Y. Oshima, Clarification of the ordering of intercalated Fe atoms in Fe$_x$TiS$_2$ and its

effect on the magnetic properties, Acta Crystallogr., B **77**, 441 (2021).

[33] T. Yoshioka and Y. Tazuke, Magnetic properties of Fe_xTiS_2 system, J. Phys. Soc. Jpn. **54**, 2088 (1985).

[34] M. Inoue, M. Matsumoto, H. Negishi, and H. Sakai, Low field ac magnetic susceptibility measurements of intercalation compounds M_xTiS_2 ($M = 3d$ transition metals), J. Magn. Magn. Mater. **53**, 131 (1985).

[35] Y. Kuroiwa, M. Nishimura, R. Nakajima, H. Abe, and Y. Noda, Short-range order and long-range order of Fe atoms in a spin-glass phase and a cluster-glass phase of intercalation compounds Fe_xTiS_2, J. Phys. Soc. Jpn. **63**, 4278 (1994).

[36] G. Calvarin, J. R. Gavarri, M. A. Buhannic, P. Colombet, and M. Danot, Crystal and magnetic structures of $Fe_{0.25}TiSe_2$ and $Fe_{0.48}TiSe_2$, Rev. Phys. Appl. (Paris) **22**, 1131 (1987).

[37] Y. Kobayashi, K. Muta, and K. Asai, The Hall effect and thermoelectric power correlated with the giant magnetoresistance in modified FeRh compounds, J. Phys.: Condens. Matter **13**, 3335 (2001).

[38] N. Pérez, A. Chirkova, K. P. Skokov, T. G. Woodcock, O. Gutfleisch, N. V. Baranov, K. Nielsch, and G. Schierning, Electronic entropy change in Ni-doped FeRh, Mater. Today Phys. **9**, 100129 (2019).

[39] Y. Kuroiwa, H. Honda, and Y. Noda, Neutron magnetic scattering of intercalation compounds Fe_xTiS_2, Mol. Cryst. Liq. Cryst. **341**, 15 (2000).

[40] J. E. Greedan, Geometrically frustrated magnetic materials, J. Mater. Chem. **11**, 37 (2001).

[41] J. Q. Xiao, J. S. Jiang, and C. L. Chien, Giant Magnetoresistance in Nonmultilayer Magnetic Systems, Phys. Rev. Lett. **68**, 3749 (1992).

[42] A. F. Gubkin, E. M. Sherokalova, L. Keller, N. V. Selezneva, A. V. Proshkin, E. P. Proskurina, and N. V. Baranov, Effects of S-Se substitution and magnetic field on magnetic order in $Fe_{0.5}Ti(S, Se)_2$ layered compounds, J. Alloys Compd. **616**, 148 (2014).

[43] N. V. Selezneva, E. M. Sherokalova, A. S. Volegov, D. A. Shishkin, and N. V. Baranov, Crystal structure, magnetic state and electrical resistivity of $Fe_{2/3}Ti(S, Se)_2$ as affected by anionic substitutions, Mater. Res. Express **4**, 106102 (2017).

[44] N. V. Selezneva, N. V. Baranov, V. G. Pleshchev, N. V. Mushnikov, and V. I. Maksimov, Magnetic state and properties of the $Fe_{0.5}TiSe_2$ intercalation compound, Phys. Solid State **53**, 329 (2011).

[45] N. V. Baranov, P. N. G. Ibrahim, N. V. Selezneva, A. F. Gubkin, A. S. Volegov, D. A. Shishkin, L. Keller, D. Sheptyakov, and E. A. Sherstobitova, Layer-preferential substitutions and magnetic properties of pyrrhotite-type $Fe_{7-y}M_yX_8$ chalcogenides ($X = $ S, Se; $M = $ Ti, Co), J. Phys.: Condens. Matter **27**, 286003 (2015).

[46] J. M. Newsam, Y. Endoh, and I. Kawada, Measurement of the cation partitionings in $Fe_xV_{3-x}S_4$ ($x = 1.0$ and 2.0) by powder neutron diffraction, J. Phys. Chem. Solids **48**, 607 (1987).

[47] A. V. Powell, P. Vaqueiro, K. S. Knight, L. C. Chapon, and R. D. Sánchez, Structure and magnetism in synthetic pyrrhotite Fe7S8: a powder neutron-diffraction study, Phys. Rev. B **70**, 014415 (2004).

[48] M. Eibschütz, S. Mahajan, F. J. DiSalvo, G. W. Hull, and J. V. Waszczak, Ferromagnetism in metallic intercalated compounds Fe_xTaS_2 ($0.20 \leqslant x \leqslant 0.34$), J. Appl. Phys. **52**, 2098 (1981).

[49] E. Morosan, H. W. Zandbergen, L. Li, M. Lee, J. G. Checkelsky, M. Heinrich, T. Siegrist, N. P. Ong, and R. J. Cava, Sharp switching of the magnetization in $Fe_{1/4}TaS_2$, Phys. Rev. B **75**, 104401 (2007).

[50] N. V. Baranov, E. Bauer, R. Hauser, A. Galatanu, Y. Aoki, and H. Sato, Field-induced phase transitions and giant magnetoresistance in Dy_3Co single crystals, Eur. Phys. J. B **16**, 67 (2000).

[51] Y. Numata, K. Inoue, N. Baranov, M. Kurmoo, and K. Kikuchi, Field-induced ferrimagnetic state in a molecule-based magnet consisting of a CoII ion and a chiral triplet bis(nitroxide) radical, J. Am. Chem. Soc. **129**, 9902 (2007).

[52] T. Tsutaoka, K. Shimomura, and A. Tanaka, Irreversible magnetovolume effect in Nd_7Rh_3 single crystal, J. Magn. Magn. Mater. **323**, 3147 (2011).

[53] A. F. Gubkin, L. S. Wu, S. E. Nikitin, A. V. Suslov, A. Podlesnyak, O. Prokhnenko, K. Prokeš, F. Yokaichiya, L. Keller, and N. V. Baranov, Field-induced magnetic phase transitions and metastable states in Tb_3Ni, Phys. Rev. B **97**, 134425 (2018).

[54] H. Negishi, A. Shoube, H. Takahashi, Y. Ueda, M. Sasaki, and M. Inoue, Magnetic properties of intercalation compounds M_xTiS_2 ($M = 3d$ transition metal), J. Magn. Magn. Mater. **67**, 179 (1987).

[55] S. Giri, M. Patra, and S. Majumdar, Exchange bias effect in alloys and compounds, J. Phys.: Condens. Matter **23**, 073201 (2011).

[56] Z. Fan, A new approach to the electrical resistivity of two-phase composites, Acta Metall. Mater. **43**, 43 (1995).